Journal of Catalysis 286 (2012) 13–21

Contents lists available at SciVerse ScienceDirect

Journal of Catalysis

journal homepage: www.elsevier.com/locate/jcat

In situ study of the formation and stability of supported Pd_2Ga methanol steam reforming catalysts

Andreas Haghofer [a], Karin Föttinger [a,*], Frank Girgsdies [b], Detre Teschner [b], Axel Knop-Gericke [b], Robert Schlögl [b], Günther Rupprechter [a]

[a] Institute of Materials Chemistry, Vienna University of Technology, Getreidemarkt 9/BC/01, 1060 Vienna, Austria
[b] Department of Inorganic Chemistry, Fritz-Haber-Institute of the Max-Planck-Society, Faradayweg 4-6, 14195 Berlin, Germany

ARTICLE INFO

Article history:
Received 8 June 2011
Revised 10 October 2011
Accepted 12 October 2011
Available online 14 November 2011

Keywords:
Palladium
Gallium oxide
Intermetallic compound
Alloy
Methanol steam reforming
Methanol decomposition
In situ X-ray photoelectron spectroscopy
In situ IR spectroscopy
In situ X-ray diffraction
CO adsorption

ABSTRACT

Pd/Ga_2O_3 methanol steam reforming (MSR) catalysts were characterized in detail by utilizing a range of *in situ* techniques of varying surface sensitivity. Correlating the nature of the intermetallic Pd–Ga compound (IMC; formed upon reduction) with the corresponding activity/selectivity revealed pronounced differences. Generally, a dynamic response of the catalyst surface to the surrounding gas environment was observed. Special attention was paid to the bulk and surface stability of the Pd–Ga IMCs. Whereas the bulk was stable in O_2, decomposition of the surface occurred resulting in a partial coverage by Ga_xO_y islands. In addition, the main formation mechanism of undesired CO and therefore the reason limiting the selectivity to MSR were identified. CO was shown to have a detrimental effect on the selective Pd–Ga intermetallic compound, causing partial decomposition of the IMC to metallic Pd at the surface. Consequently, patches of Pd metal are present under reaction conditions, catalyzing the unwanted parallel methanol decomposition reaction.

1. Introduction

Hydrogen is considered as one of the most promising and clean energy carriers of the future, especially in combination with fuel cells. It can be produced from a variety of resources including bio-feedstock. One of the major processes for hydrogen production is steam reforming of hydrocarbons or oxygenates. Among the latter, methanol is especially interesting for on-board production of hydrogen [1–5], since it is easy to store, transport, and handle.

Cu-based catalysts are highly active and selective for methanol steam reforming [2,6–9]. High selectivity to CO_2 and H_2 production is crucial due to the poisoning effect of CO on fuel cell anodes in polymer electrolyte membrane fuel cells (PEMFC), requiring <20 ppm CO in the H_2 fuel [10]. Pd supported on ZnO has attracted much attention due to its superior stability compared with Cu/ZnO [3,11,12]. In contrast to Pd on inert supports such as SiO_2 or active carbon, which catalyzes methanol decomposition to CO and H_2 [13], Pd on ZnO, Ga_2O_3, and In_2O_3 can show high activity and selectivity for steam reforming to CO_2 and H_2 [14,15].

Several explanations were proposed for the remarkable alteration in the catalytic properties on certain supports, such as the formation of Pd–Zn, Pd–Ga, and Pd–In alloys. By XPS and UPS valence band studies, it was found that the electronic properties of the 1:1 PdZn alloy resemble those of metallic Cu [16,17], which was confirmed by DFT density of states calculations [18,19]. Using DFT, Neyman et al. [18] calculated reaction barriers for methoxy dehydrogenation to CO and H_2 on Pd, PdZn, and Cu surfaces and found similar barriers for the dehydrogenation of intermediate formaldehyde to CO on Cu and PdZn, which are both notably higher than on Pd. These findings could explain the excellent selectivity of PdZn to MSR, similar to Cu.

While several research groups studied Pd/ZnO MSR catalysts, less work was dedicated to Pd/Ga_2O_3. Pd and Ga can form a number of intermetallic compounds (IMC) and/or alloys; e.g., Pd_2Ga, PdGa, Pd_3Ga_7, and $PdGa_5$ were reported in literature [20]. Metallurgically prepared, unsupported intermetallic bulk materials have been studied in recent years, showing excellent catalytic properties for selective hydrogenation of acetylene in excess ethylene [21–24].

Ga_2O_3 on its own exhibits interesting catalytic properties as well, e.g., Ga_2O_3 supported on zeolites is active in the dehydrogenation and aromatization of light alkanes [25–28]. Recently, the

* Corresponding author. Fax: +43 1 58801 165980.
E-mail address: karin.foettinger@tuwien.ac.at (K. Föttinger).

0021-9517/$ - see front matter © 2011 Elsevier Inc. All rights reserved.
doi:10.1016/j.jcat.2011.10.007

influence and role of oxygen defects on β-Ga_2O_3 samples was investigated for the (reverse) water–gas shift reaction [29,30] by systematically studying the interaction with H_2, CO_2, CO, and H_2O after different pretreatments. In another work, Ga_2O_3 supported on TiO_2 showed remarkable activity for steam reforming of dimethylether [31]. Bonivardi and coworkers [32] studied the interaction of Ga_2O_3 and Pd/Ga_2O_3 with H_2 and CO_2 for methanol synthesis. In contrast to Iwasa's work, they did not observe Pd–Ga alloy formation [33]. They attributed the catalytic activity for methanol synthesis to the reaction of polydentate carbonates with dissociatively adsorbed hydrogen on the Ga_2O_3 surface, while the addition of Pd only accelerates the reaction by spillover of hydrogen [32]. Penner et al. [34] and Lorenz et al. [35], however, did observe Pd–Ga alloying and improved selectivity in steam reforming in a study focusing on Pd/Ga_2O_3 thin-film model catalysts, but identified different intermetallic compounds than Iwasa's group.

By utilizing a range of *in situ* techniques with varying bulk and surface sensitivities, we have explored in detail the structure, electronic properties, available surface sites, and catalytic properties of Pd/Ga_2O_3 MSR catalysts under pretreatment and reaction conditions. Questions that were addressed include which phase forms during H_2 reduction as well as under actual MSR conditions and what is the stability of the intermetallic phases formed in different atmospheres. Special attention was paid to combining information on surface and bulk properties of the materials. The characterization and stability data were correlated with the catalytic properties to identify the pathways leading to the formation of residual unwanted CO.

2. Experimental

2.1. Materials

Ga_2O_3-supported Pd catalysts were prepared by incipient wetness impregnation of commercial β-Ga_2O_3 (Alfa Aesar, 99.99% purity, particle size <250 μm). The Ga_2O_3 surface area was determined by the adsorption of N_2 according to BET and amounted to 7 m^2/g. Metal loadings of 2 and 5 wt.% were prepared by varying the amount of palladium(II) acetate (Fluka) precursor dissolved in toluene (Merck, p.a.). After impregnation, the catalysts were dried at 373 K for 48 h and subsequently calcined at 773 K for 4 h in static air. Reduction of the catalysts was performed *in situ*, except for transmission electron microscopy measurements for which samples were reduced externally.

2.2. In situ X-ray diffraction (XRD)

In situ XRD experiments were performed on a STOE Theta/Theta diffractometer (Cu Kα radiation, secondary monochromator, and scintillation counter) operating in reflection scan mode. The diffractometer is equipped with an Anton Paar XRK 900 high-temperature gas cell. *In situ* diffraction patterns were recorded in a 2θ range from 32.5° to 47.5° with a step size of 0.02° and a time per step of 2 s. The calcined sample (5 wt.% Pd/Ga_2O_3) was preoxidized at 773 K in a 20% O_2/He mixture, then cooled to 303 K, and flushed in He. The atmosphere was then changed to a flow of 25% H_2 in He, and the diffraction pattern was recorded. To check for the presence of Pd–hydride, the cell was subsequently flushed in He once more before starting the temperature-programmed reduction in H_2/He from 303 K to 773 K with diffractograms being recorded at temperature plateaus in steps of 25 K. An analogous temperature-programmed experiment was performed in the absence of H_2, i.e., in a flow of pure He. All experiments were performed at ambient pressure at a total flow of 100 ml/min.

2.3. Transmission electron microscopy (TEM)

Transmission electron micrographs were acquired with a 200 kV FEI TECNAI F20 S-TWIN analytical transmission electron microscope, equipped with a field emission source. TEM specimens were prepared by dipping a holey carbon–coated copper grid into the fine sample powders. Before microscopy, catalyst samples were reduced (*ex situ*) in a H_2 flow for 120 min. Reduction temperatures were 303 K and 673 K.

2.4. In situ X-ray photoelectron spectroscopy (XPS)

In situ XP-spectroscopy experiments were performed at the ISISS beamline at BESSY II (Helmholtz-Zentrum Berlin) at photon energies between 160 and 1120 eV and normal electron emission. The setup allows for *in situ* photoemission studies in the mbar range and has been described in detail, e.g., in [36]. Hydrogen and oxygen gas were introduced into the system by calibrated mass flow controllers. All spectra were corrected for synchrotron beam current, incident photon flux, and energy-dependent photoionization cross sections [37]. Binding energy calibration, to account for small shifts due to sample charging, was done by keeping the main Ga^{3+} signal originating from the bulk Ga_2O_3 support at 20.55 eV and additionally recording valence band spectra at the same excitation energy. Peak deconvolution was performed using the software XPSPeak 4.1 by fitting symmetric Gauss–Lorentz sum functions with the exception of Pd metal for which an asymmetric peak shape was used (described by the parameters TS (peak shape asymmetry) and TL (tail extension asymmetry)).

2.5. In situ FTIR spectroscopy

FTIR spectra were recorded in transmission mode on a Bruker IFS 28 spectrometer using an MCT detector at a resolution of 4 cm^{-1}. The calcined samples were pressed into self-supporting wafers (6 mm in diameter, $m \approx 10$ mg) and placed into a small transmission flow cell with CaF_2 windows, equipped with a ring-shaped furnace and a type-K thermocouple mounted to the sample holder. A spectrum recorded without sample in a flow of He was used as a background that was subtracted from all spectra. Typically, about 100 scans were summed up, so that recording an IR spectrum took less than 1 min. All pretreatments were performed *in situ* inside the cell using gas flows introduced via calibrated mass flow controllers.

In the temperature-programmed reduction experiment, the sample was reduced for 60 min in 25% H_2/N_2 at each temperature ranging from 303 K to 673 K (the maximum temperature in the current cell construction), flushed, and cooled to room temperature in pure N_2 before switching to the 5% CO/He mixture (p_{CO} = 50 mbar) used for adsorption. Before reduction at the next (higher) temperature, CO was removed from the surface by heating to 673 K in a flow of N_2.

In the *in situ* experiment performed under methanol steam reforming turnover, the sample was reduced at 303 K and 673 K in an analogous way, then flushed in pure N_2 at 673 K, and cooled to the desired reaction temperature before switching to the steam reforming feed containing CH_3OH and H_2O at a molar ratio of 1:1 (p_{CH3OH} = p_{H2O} = 10 mbar).

2.6. Catalytic measurements

Methanol steam reforming (MSR) and reverse water–gas shift (RWGS) studies were carried out in a continuous fixed-bed flow reactor (d = 4 mm) at reaction temperatures between 493 and 573 K and atmospheric pressure. All gases were introduced via calibrated mass flow controllers. In MSR, separate He flows were

channeled through saturators containing liquid methanol and water, resulting in a molar $CH_3OH:H_2O$ ratio of 1:1 ($p_{CH3OH} = p_{H2O} = 30$ mbar) at a total flow of 20 ml/min. In RWGS, the reaction mixture contained H_2 and CO_2 at a molar ratio of 3:1 ($p_{CO2} = 18$ mbar, $p_{H2} = 54$ mbar) at a total flow of 40 ml/min. The resulting mixture in each case was fed to a temperature-controlled, fixed-bed reactor containing 20 mg of catalyst and was subsequently analyzed by a HP6890 gas chromatograph, equipped with a HP Plot Q column, a nickel catalyst methanizer, and a flame ionization detector.

3. Results and discussion

3.1. Bulk structure upon reduction

3.1.1. In situ X-ray diffraction

To determine the Pd–Ga phases formed during the reduction of the Pd/Ga_2O_3 powder catalyst and to correlate them later with catalytic properties, X-ray diffraction experiments were performed *in situ* during heating in a flow of 25% H_2 in He (Fig. 1). Reflections originating from the crystalline β-Ga_2O_3 support remained unchanged, regardless of the temperature and atmosphere, and are marked by full circles in Fig. 1. At temperatures from 398 to 523 K, the 1 1 1 reflection of Pd metal at $2\theta = 40.2°$ was additionally observed. Up to 348 K, in H_2/He (diffractogram not shown), Pd–β-hydride ($2\theta \approx 38.5°$) was present, and thus the Pd metal 1 1 1 reflection was only observed upon removal of H_2 from the analysis chamber (bottom diffractogram in Fig. 1). Above 523 K, the Pd 1 1 1 reflection disappeared and reflections at $2\theta = 44.6°$, 41.2°, 40.1°, and 39.7° assigned to the intermetallic Pd_2Ga phase [34,38] appeared gradually. During reduction between 623 and 673 K, Pd_2Ga is stable according to XRD. Increasing the reduction temperature further up to 773 K led to the formation of the Ga-richer intermetallic compound PdGa [34] (top diffractogram in Fig. 1). Regarding their bulk structure, both compounds proved to be stable in air at room temperature. The intermetallic compounds identified as well as their approximate formation temperatures observed *in situ* agree reasonably well with previous *ex situ* studies by Penner et al. [34] but are in variance to a study by Iwasa et al. [15], who observed a similar XRD pattern upon reduction of a 10 wt.% Pd/Ga_2O_3 catalyst at 773 K, but interpreted it as a mixture of Pd_5Ga_2 and $PdGa_5$. After careful analysis of our data, we see no indication of the presence of a mixture of Pd–Ga phases. Rietveld refinement using only Ga_2O_3 and Pd_2Ga was able to model the experimental diffractogram after reduction at 673 K well. Also it appears likely that higher reduction temperatures are needed to form a phase that is as rich in Ga as $PdGa_5$.

Additionally, an analogous temperature-programmed experiment was performed in pure He (in the absence of H_2), in which Pd remained in a metallic state up to 773 K and no formation of any intermetallic compound was observed.

3.1.2. Transmission electron microscopy

Transmission electron microscopy was performed following reduction of the Pd/Ga_2O_3 at 303 K and 673 K to determine the changes in particle size and morphology upon the formation of the Pd_2Ga intermetallic compound. Exemplary micrographs are shown in Fig. 2a for the 303 K-reduced sample (i.e., Pd particles on Ga_2O_3 according to XRD) and Fig. 2b for the 673 K-reduced sample (i.e., Pd_2Ga particles on Ga_2O_3 according to XRD). From the analysis of TEM micrographs, it becomes evident that strong morphology changes and sintering do not occur upon reduction at 673 K and intermetallic formation. The average particle size increases from 4.1 ± 1.2 nm to 4.9 ± 1.4 nm. This is reasonably close to the expected 1.5-fold volume increase upon incorporation of Ga into Pd and formation of the orthorhombic Pd_2Ga phase. This corroborates the absence of strong morphology and size changes upon the formation of the bimetallic phase and thus enables us to compare the intrinsic catalytic properties of the supported intermetallic with those of the unalloyed Pd particles excluding strong size and morphology effects.

3.2. Electronic structure and surface composition during reduction and reaction

In situ XRD allowed investigating the formation of bulk crystalline intermetallic particles during (temperature-programmed) reduction. However, a modified surface layer is generally sufficient to drastically alter catalytic properties; therefore, we used *in situ* techniques with various degrees of surface sensitivity to follow changes in electronic structure, surface composition, and adsorption sites during reduction in H_2 as well as under methanol steam reforming reaction conditions.

3.2.1. In situ XPS during H_2 reduction

Synchrotron radiation–based high-pressure XPS was used to follow changes in the near-surface electronic structure of the Pd/Ga_2O_3 catalyst that result from the bulk structural transition observed in XRD. The main interest was on the binding energy regions from 16 to 26 eV covering Ga 3d and from 332 to 339 eV covering Pd 3d signals. To obtain equal information depth for Ga 3d and Pd 3d core levels, corresponding pairs of excitation energies were chosen (as listed in Table 1) leading to equal kinetic energies of the emitted photoelectrons.

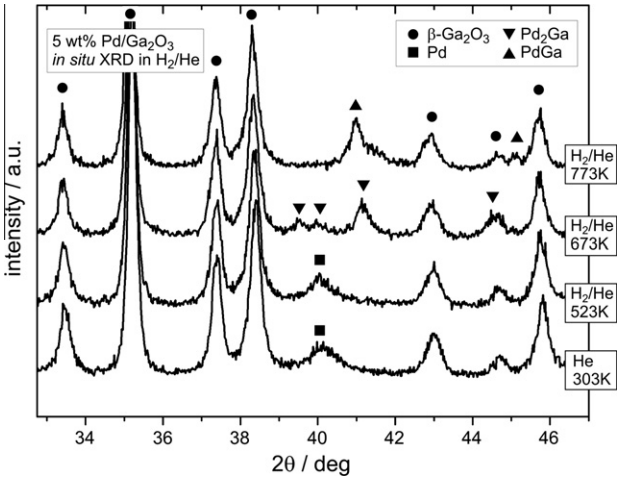

Fig. 1. *In situ* X-ray diffractograms of 5 wt.% Pd/Ga_2O_3 during reduction in H_2/He at the indicated temperature.

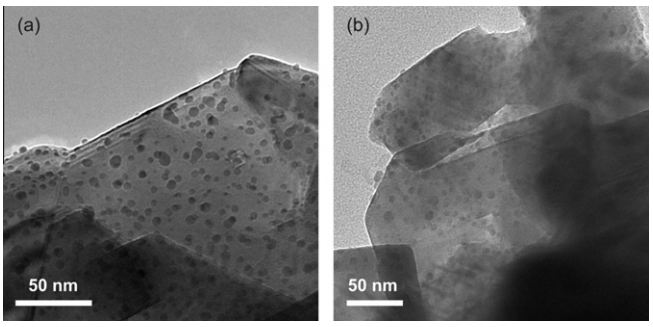

Fig. 2. Transmission electron micrographs of Pd/Ga_2O_3 reduced at (a) 303 K and (b) 673 K.

Table 1
Excitation energies and resulting photoelectron kinetic energies for Pd 3d and Ga 3d core levels with corresponding inelastic mean free paths in Pd. Atomic ratios of Pd to zero-valent Ga during reduction at 623 K at varying surface sensitivity.

Excitation energy (eV)		Kinetic energy (eV)	Inelastic mean free path (Pd) [57] (Å)	Atomic ratio Pd:Ga^0
Pd 3d	Ga 3d			
1120	800	≈780	15	2.0 ± 0.5
720	400	≈380	9	2.2 ± 0.3
480	160	≈140	5	3.1 ± 0.4

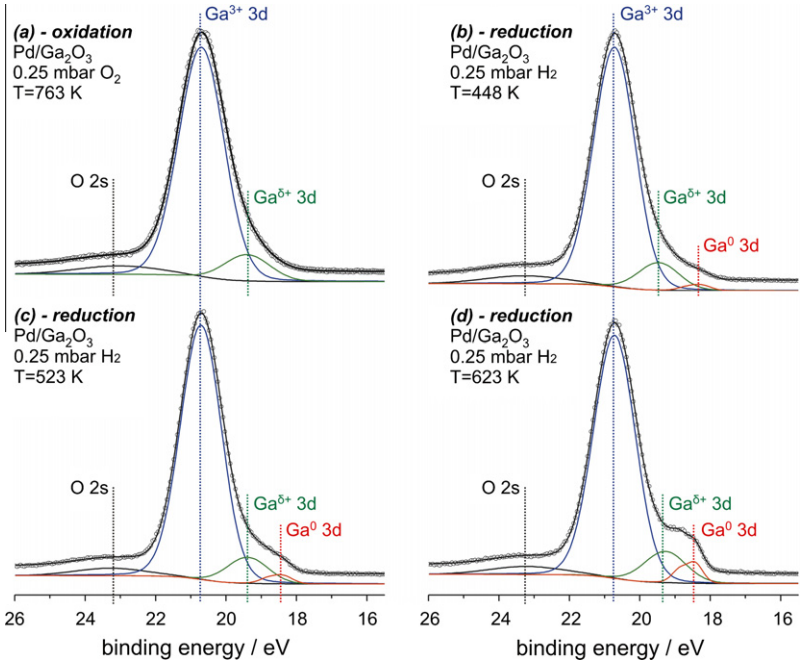

Fig. 3. Ga 3d region of Pd/Ga_2O_3 recorded *in situ* during oxidation in 0.25 mbar O_2 at 723 K (a) and during reduction in 0.25 mbar H_2 at 448 K (b), 523 K (c), and 623 K (d).

Generally, spectra recorded at different excitation energies turned out to be similar. Therefore, mainly the spectra recorded at medium surface sensitivity $E_{kin} \approx 380$ eV will be discussed. Cases in which discrepancies were observed between the excitation energies are mentioned separately. Two different samples were analyzed, the 5 wt.% Pd/Ga_2O_3 catalyst and the pure Ga_2O_3 support. Both samples were preoxidized at 723 K in 0.25 mbar O_2, cooled to 623 K in O_2, further cooled to 373 K in vacuum, and then exposed to 0.25 mbar H_2 at increasing temperature up to 623 K.

Fig. 3 shows the Ga 3d binding energy region recorded on Pd/Ga_2O_3 during preoxidation (a) and during reduction at 448 (b), 523 (c), and 623 K (d). The main signal at 20.55 eV remained unchanged, irrespective of the atmosphere and temperature, and can unambiguously be assigned to Ga^{3+} from the Ga_2O_3 support [39]. A broad O 2s signal also originating from the Ga_2O_3 support was additionally observed at around 23 eV and proved to be independent of atmosphere and temperature. As expected, both the Ga and the O signals were observed on the pure Ga_2O_3 support as well (cf. Fig. 4).

A signal at binding energies of 19.2 ± 0.1 eV (ΔBE = −1.35 ± 0.10 eV relative to Ga^{3+}) was observed on the Pd catalyst, both under oxidative and under reductive conditions (see Fig. 3), and is assigned to Ga in an intermediate oxidation state ($Ga^{\delta+}$, $\delta < 2$) [33,39]. On supported Ga/SiO_2 and Ga–Pd/SiO_2 catalysts, a signal at the same relative position (ΔBE = −1.2 to −1.4 eV compared with Ga^{3+}) was observed only upon high-temperature reduction and interpreted as incompletely reduced Ga at the surface [33]. In our case, an assignment of the band to intrinsic oxygen defects within the oxide is more likely, due to the presence of the signal in similar intensity under reductive and oxidative conditions. The Gaδ+ signal was observed not only on the Pd/Ga_2O_3 catalyst, but also in similar intensity on the pure Ga_2O_3 support (see Fig. 4), further supporting our assignment as an oxygen defect–related species.

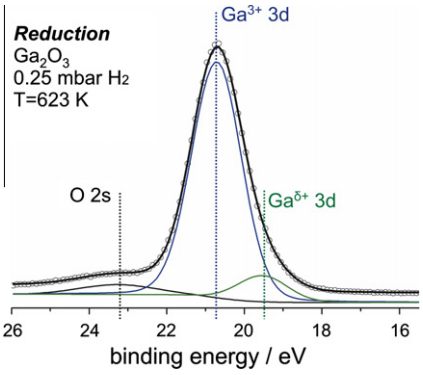

Fig. 4. Ga 3d region of pure Ga_2O_3 support recorded *in situ* during reduction in 0.25 mbar H_2 at 623 K.

Fig. 3b clearly shows that during reduction of Pd/Ga_2O_3 at 448 K, an additional photoelectron peak was observed at 18.35 ± 0.10 eV. Since the observed chemical shift of 2.2 eV between Ga^{3+} and the low-energy Ga species is in the range reported in the literature for oxidic and metallic Ga [39,40], and in

Table 2
Atomic ratios of Ga species of various oxidation states on Pd/Ga_2O_3 during calcination, during reduction at 448, 523, and 623 K and during subsequent reoxidation. E_{exc} = 400 eV.

Step #	Atmosphere	Temp. (K)	Atomic ratios $Ga^{\delta+}$:Ga^{3+}	Ga^0:Ga^{3+}
1	Oxidation in 0.25 mbar O_2	763	0.12 ± 0.02	<0.005
2	Reduction in 0.25 mbar H_2	448	0.12 ± 0.02	0.02 ± 0.01
3	Reduction in 0.25 mbar H_2	523	0.10 ± 0.02	0.02 ± 0.01
4	Reduction in 0.25 mbar H_2	623	0.13 ± 0.02	0.05 ± 0.01
5	Reoxidation in 0.25 mbar O_2	723	0.12 ± 0.02	<0.005

accordance with *in situ* XRD, we assign this species to zero-valent Ga within the intermetallic compound Pd_2Ga. XPS studies of bulk, metallurgically prepared PdGa (1:1 composition) additionally support our peak assignment [23]. The lower onset-temperature of intermetallic formation compared with XRD can be explained by the surface sensitivity of XPS, which in contrast to XRD does not rely on the presence of three-dimensional crystalline intermetallic particles of a certain size. Further implications of this are discussed in Section 3.2.2. As the reduction temperature was increased to 523 and 623 K, the intensity of the Ga^0 species increased (see Fig. 3c and d and Table 2) up to a relative amount of about 5% Ga^0 within the investigated surface region at 623 K. Obviously, as expected due to the Pd loading of only 5 wt.%, the majority of Ga in the Ga_2O_3 support remains in the 3+ oxidation state. Depth profiling during reduction at 623 K revealed equal relative amounts of Ga^0 at all three information depths, indicating that the reduced Ga species is distributed uniformly over the depth range accessed by the experiment.

Reduction of the pure Ga_2O_3 support at the same temperature clearly did not lead to the formation of any metallic Ga (Fig. 4). This indicates a promoting role of Pd (through hydrogen dissociation) in the reduction to zero-valent Ga that must precede the intermetallic compound formation. Generally, the observed XPS peak positions and shapes relate well to measurements on the metallurgically prepared, unsupported intermetallic compound PdGa [23] and on Ga/Ga_2O_3 thin films [40], which both showed a resolvable doublet for (inter)metallic Ga and broader peaks for the oxidized component at similar binding energies.

A photoelectron spectrum of the Pd 3d region of the Pd/Ga_2O_3 catalyst during reduction in 0.25 mbar H_2 at 623 K and 448 K is depicted in Fig. 5a and b, respectively. During reduction at 448 K, the Pd $3d^{5/2}$ signal exhibited an overall maximum at a binding energy of 335.4 eV. Its large FWHM of 1.3 eV indicates the presence of more than one Pd species. In accordance with the Ga 3d spectra that showed small amounts of zero-valent Ga at this reduction temperature, this indicates the co-existence of metallic Pd and of Pd interacting with zero-valent Ga at a beginning stage of intermetallic formation. It was possible to fit the Pd 3d region using two species: an asymmetric one (TS = 0.1, TL = 40) at a binding energy of 335.2 eV and a symmetric one at 335.7 eV, with the former value being characteristic of metallic Pd particles of the nm size regime [41–43]. The latter higher BE is similar to that of Pd 3d observed in unsupported bulk intermetallic Pd–Ga compounds [23] and, in combination with XRD, we therefore assign it to Pd within the IMC Pd_2Ga. Additionally, a broad peak at approximately 342 eV is present and can be assigned to a Plasmon excitation shifted by about 6.5 eV compared with Pd $3d^{5/2}$ [44].

Upon increase in the reduction temperature to 623 K, only the Pd $3d^{5/2}$ signal assigned to Pd within Pd_2Ga remained and now appeared at 335.8 eV. The FWHM of 0.9 eV indicates that only one Pd species is present at this point, i.e., during reduction at 623 K, all Pd on the surface formed Pd_2Ga with reduced Ga from the support. Additionally, the plasmon excitation at around 342 eV has

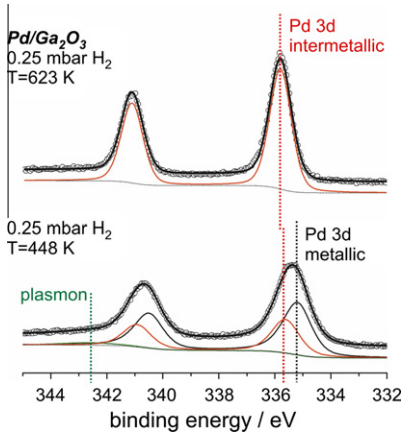

Fig. 5. Pd 3d region recorded *in situ* during reduction in 0.25 mbar H_2 at 448 and 623 K. The additional small peak at ≈342 eV corresponds to a plasmon excitation shifted by about 6.5 eV relative to the Pd $3d^{5/2}$ signal [44].

vanished. These observations are a clear indication of the major electronic changes [45] that have apparently occurred during the formation of the intermetallic compound. Taking into consideration the different energy-dependent cross sections for Pd 3d and Ga 3d core levels [37] at the respective excitation energies, a calculation of atomic Pd:Ga^0 ratios yielded values of about 2:1 for the two less surface-sensitive excitation energies (cf. Table 1). This agrees with the expected ratio for Pd_2Ga within the accuracy of the method. The deviation of the ratio in the most surface-sensitive mode is a known issue in XPS-derived atomic ratios when using very low excitation (and kinetic) energies and was also observed for the Ga:O ratio on pure Ga_2O_3.

From *in situ* XPS measurements, we thus conclude that the activation of hydrogen occurs on Pd that is, according to XRD, fully reduced already at 303 K. Hydrogen spillover to Ga_2O_3 then leads to partial support reduction followed by intermetallic compound formation, likely starting at the perimeter of the particle–support interface. A promotional reduction effect of the noble metal through hydrogen spillover from metallic palladium has also been suggested by Collins et al. [33] for $Ga–Pd/SiO_2$ catalysts. However, in contrast to our work, no Ga is in metallic state, and therefore no intermetallic compound or alloy was observed.

In order to assess the stability of the intermetallic compound under oxidative conditions, the Pd/Ga_2O_3 sample was subsequently exposed to 0.25 mbar O_2 at 723 K for 10 min. We observed the disappearance of the Ga^0 signal indicating decomposition of the intermetallic compound and reoxidation of the incorporated zero-valent Ga in the XPS-probed surface region. Additionally, the Pd 3d signal decreased in intensity by 60% and, although Pd(1 1 1) and supported nanoparticles have been shown to form PdO (E_b > 336 eV) at comparable conditions [44,46,47], Pd remains in a metallic state. These observations point to the formation of a Ga_xO_y overlayer or islands on the particle surface during oxidative decomposition of the intermetallic. We have recently proposed a similar model for supported PdZn particles [48].

3.2.2. IR spectroscopy of adsorbed CO upon H_2 reduction

To investigate the changes in the outermost surface layer during intermetallic formation, we have utilized the ultimate surface sensitivity of IR spectroscopy when probing adsorbed CO. Fig. 6a–d shows spectra obtained upon adsorption of CO following reductive treatment at temperatures from 303 K to 673 K.

Reduction of the catalyst at 303 K and subsequent adsorption of CO yielded a spectrum with a C–O stretching region typical of CO adsorbed on metallic Pd particles in the low-nm-size regime

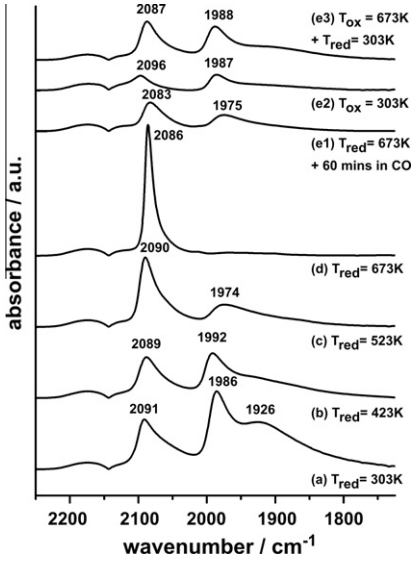

Fig. 6. CO stretch region of IR spectra recorded upon CO adsorption after reduction at temperatures from 303 K to 673 K (a–d) and upon keeping the 673 K-reduced sample in 50 mbar CO for 60 min (e1). Spectra (e2) and (e3) were recorded upon reoxidation at 303 K (e2) and upon reoxidation at 673 K and subsequent reduction at 303 K (e3) of a freshly 673 K-reduced sample. All adsorption experiments were performed at 298 K in a partial pressure of 50 mbar CO in He.

[49,50]. This is in agreement with XRD measurements which showed that reduction at room temperature is sufficient to reduce the initially present PdO (from calcination) to metallic Pd. Besides the obvious contribution of gas-phase CO with a minimum at 2143 cm^{-1}, we observed three distinct bands in the carbonyl region. The signal at 2091 cm^{-1} can be assigned to CO adsorbed linearly on metallic Pd atoms, the one at 1986 cm^{-1} to bridge-bonded CO on edges/steps or (1 0 0) facets and the one at 1926 cm^{-1} corresponds to hollow- or bridge-bonded CO on (1 1 1) facets [42,49].

Reduction of the catalyst at temperatures of 423 and 523 K and subsequent adsorption of CO already indicate pronounced changes in the outermost surface layer of the (inter)metallic particles. The amount of bridge- and hollow-bonded CO species (as estimated from peak areas) initially decreased with increasing reduction temperature indicating a beginning intermetallic formation. This is in agreement with *in situ* XPS results that showed some zero-valent Ga and electronically modified Pd during reduction at 448 K. The lower-onset temperature of intermetallic formation compared with *in situ* XRD can be readily explained by the surface sensitivity of IR spectroscopy (and XPS) in this case. While XRD can only detect intermetallic particles once they are crystalline and of a certain size, IR spectroscopy is sensitive to CO adsorbed on intermetallic particles that can be (a) very small and (b) in an early stage of intermetallic formation where no crystalline compound has yet formed while the particle surface is already modified (alloyed). The low reduction temperatures required to modify the outermost surface layer that is probed by IR spectroscopy is an indication that the intermetallic formation indeed begins at the particle surface (as for the Pd/ZnO system [48]).

Finally, upon reduction of the catalyst at 623 K (not shown) and 673 K, bridge- and hollow site-bonded CO species almost completely disappeared from the spectrum, accompanied by an intensity increase of the linearly bonded CO species that appeared at 2086 cm^{-1}. This indicates now in agreement with XRD, that the formation of the intermetallic compound Pd_2Ga is completed during hydrogen treatment at this temperature.

Generally, changes in the adsorption properties of alloys with respect to the pure metal are rationalized following two lines of argument: (i) geometric "ensemble effects" referring to the fact that ensembles of specific (in this case Pd) adsorption sites are no longer available and (ii) electronic "ligand effects", referring to neighboring atoms of a different element (in this case Ga) modifying the electronic structure of the adsorbing atom (in this case Pd) in a way that changes the adsorption properties with respect to CO (or any other adsorbate) [50,51]. In the case of Pd_2Ga, the formation of a Pd–Ga alloy or intermetallic compound is mainly manifested by a low binding energy of CO in bridge and hollow sites, whereas only a small shift of the on-top CO band was observed. Although no complete isolation of Pd atoms from each other can be expected from the crystal structure of Pd_2Ga, the nearest Pd–Pd distance is somewhat increased compared with Pd metal [38]. Bridge-bonded CO has been shown to occur less frequently in transition metal complexes with larger metal–metal spacing [52]. Apparently, the increase is sufficient to destabilize bridge- and hollow-bonded CO on Pd_2Ga and achieve site isolation to some extent. Comparable studies of supported PdZn intermetallic compounds [11,53] and Pd–Ag [54,55] alloys reported a similar picture regarding reduced amounts of multiply bonded species but with red shifts of the linear CO band of 20–40 cm^{-1}. CO adsorption on metallurgically prepared bulk PdGa intermetallic compound reported even stronger shifts, down to as far as 2047 cm^{-1} [23]. In PdGa (1:1 composition), however, the crystal structure predicts a complete isolation of Pd atoms by Ga atoms; therefore, a stronger electronic (=ligand) effect of Ga on individual Pd atoms can be expected.

3.2.2.1. Stability of the intermetallic surface. The stability of the intermetallic surface was evaluated (i) under high pressures of CO (50 mbar) employed during adsorption experiments, (ii) upon exposure to synthetic air at 303 K, and (iii) upon reoxidation at 673 K and subsequent 303 K reduction.

Ad (i): It was observed that when keeping the catalyst in 50 mbar of CO for a longer period of time up to 1 h, a signal at 1975 cm^{-1} appeared with increasing intensity that can again be assigned to multiply coordinated CO. Additionally, the peak assigned to linearly bonded CO at 2086 cm^{-1} lost intensity and was shifted to 2083 cm^{-1}, finally leading to the spectrum depicted in Fig. 6(e1). Apparently, the intermetallic compound exhibits isolated adsorption sites initially, but its surface seems to respond to CO exposure in a way that suggests an (at least partial) breakup of the intermetallic compound into surface regions containing metallic Pd (as indicated by the presence of bridging CO species). Repeated reduction cycles show the same effect again, i.e., spectrum (d) in Fig. 6 is again observed initially and the intermetallic again breaks up upon longer exposure to CO.

Ad (ii): Exposing the 673 K-reduced catalyst to synthetic air at 303 K and subsequently adsorbing CO results in the spectrum depicted in Fig. 6(e2). Apparently, contrary to the bulk stability observed in XRD, the intermetallic *surface* is modified by exposure to air already at room temperature. A spectrum indicative of metallic Pd is observed. However, the overall intensity of the observed IR bands is much smaller than before. Since sintering is not an issue according to TEM, and any chemisorbed O from the oxidative treatment is easily reacted away by coadsorbed CO at 303 K [56], this indicates that the metallic Pd surface is not simply restored after oxygen exposure, as is the case for supported PdZn particles [11]. Rather, we suggest that during the decomposition of the intermetallic particles in oxygen, Ga segregates from surface near regions to the outermost layer, is then oxidized, and covers parts of the particle surface. This is also supported by the intensity decrease we observed in Pd 3d XPS during reoxidation (see Section 3.2.1).

Ad (iii): A more severe oxidative treatment (at 673 K) followed by reduction at 303 K shows a similar picture regarding the decomposition of the intermetallic surface (see Fig. 6 (e3)), again

in agreement with XPS data, but still does not fully regenerate the monometallic Pd surface (cf. Fig. 6a).

3.2.3. In situ IR under methanol steam reforming conditions

In situ IR spectroscopy during methanol steam reforming (MSR) on Pd/Ga_2O_3 was used to gain information on the composition of the outermost surface layer under reaction conditions. Pretreatment was chosen according to the two distinct cases determined from XRD and IR spectroscopy, namely reduction at 303 K and reduction at 673 K. Therefore, the state of the catalyst before MSR reaction represents either supported particles of metallic Pd or intermetallic Pd_2Ga, respectively. Fig. 7 shows the CO stretch vibration region of IR spectra recorded during MSR at temperatures of 430, 455, and 480 K, (a) after reduction at 303 K and (b) after reduction at 673 K. All spectra in Fig. 7 were recorded after about 30 min time on stream; however, no spectral changes with time were observed within these 30 min of reaction. In both cases, enough CO is formed during reaction, to serve as a probe molecule that is detected in the spectra. Similar to the spectra recorded in CO only (Fig. 6), pronounced differences are observed in the carbonyl region, already confirming that the modified surface composition achieved by high-temperature reduction is at least partly maintained under reaction conditions. In the spectra in Fig. 7a, once again the typical spectrum of CO on metallic Pd particles is observed. Obviously, the IR acquisition temperature is higher now and also the CO pressure is smaller than during adsorption in the previous section (a CO partial pressure of lower than 1.3 mbar can be estimated from the rate of CO production under these conditions). Still the bands are the same as those in Fig. 6a, only shifted to smaller wavenumbers, an effect of lower coverage at higher temperature and lower CO pressure. Linearly bonded CO shows a maximum at 2056 cm^{-1}; bridge-bonded CO on edges/steps or (100) facets is found at 1968 cm^{-1} and hollow/bridge-bonded CO on (111) facets is found at ≈1920 cm^{-1}. It should be noted that the spectrum remains unchanged up to the maximum reaction temperature of 480 K, which indicates that despite the H_2 formed as a reaction product and despite the elevated temperature, no detectable intermetallic formation takes place under these reaction conditions.

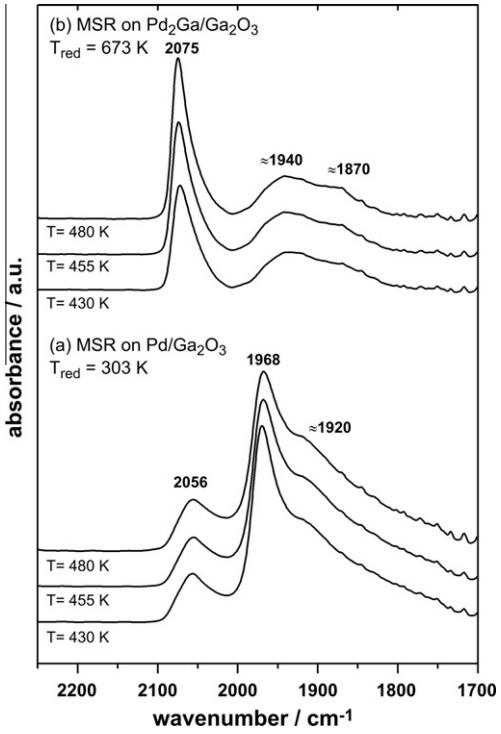

Fig. 7. CO stretch region of IR spectra recorded *in situ* during methanol steam reforming (MSR) reaction at temperatures of 430, 455, and 480 K after reduction at 303 K (a) and 673 K (b). $p_{CH3OH} = p_{H2O} = 10$ mbar, total flow = 40 ml/min.

The spectra in Fig. 7b represent the *in situ* IR spectrum of the catalyst after high-temperature reduction, at an estimated CO pressure of below 0.2 mbar. The main band appears at 2075 cm^{-1} here (cf. Fig. 6) and a notable amount of multiply bonded CO is detected, indicating that under MSR reaction conditions, part of the surface consists of metallic Pd. This implies that part of the intermetallic surface formed during reduction does not seem to be stable under MSR reaction conditions, which consequently may be the reason for the incomplete suppression of CO formation, as discussed in Section 3.3.

3.3. Catalytic measurements and structure–activity correlations

By combining the *in situ* structural information derived from XRD and the surface-sensitive information from XPS and CO-IR with reactivity measurements in a plug-flow reactor, a clear correlation between the catalyst state and its catalytic properties in methanol steam reforming (MSR) can be drawn. The left side of Fig. 8 shows the development of CO_2 selectivity with increasing reduction temperature, up to a maximum of about 90% upon complete formation of Pd_2Ga. The pronounced changes in selectivity are accompanied by an increase in the conversion of CH_3OH; however, additional experiments in which a wide range of conversions was studied by (i) decreasing and then again increasing reactor temperature and (ii) varying the reactant flow rate at constant reactor temperatures (see Fig. S1, Supplementary material) have shown that the selectivity is not influenced by the conversion and is therefore characteristic of the state of the surface of the catalyst (metallic or intermetallic). Using the TEM-derived particle sizes, methanol turnover frequencies per surface Pd atom can be calculated under the assumption of a spherical particle shape and a stoichiometric composition of the Pd_2Ga surface. In the two distinct cases of the fully metallic (T_{red} = 303 K) and the fully intermetallic (T_{red} = 673 K) catalyst, turnover frequencies are 0.03 and

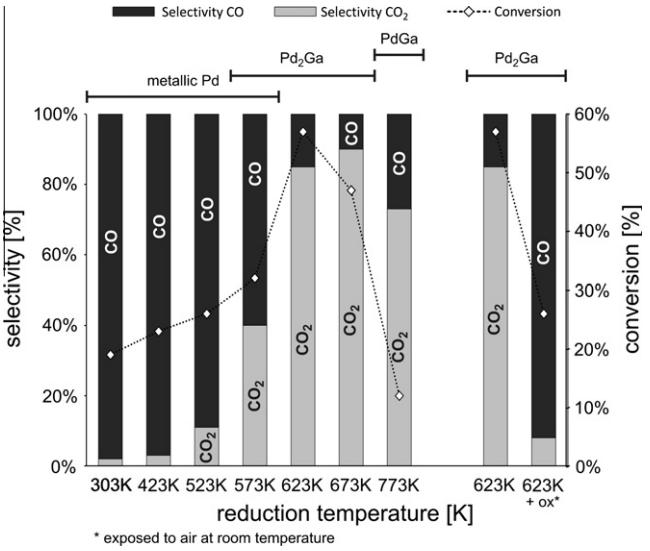

Fig. 8. Initial selectivity (bars) and total reaction rate (diamonds) during methanol conversion over Pd/Ga_2O_3 as function of the reduction temperature (left). The effect of air exposure on selectivity and total rate is shown on the right. Ranges on the top mark phases detected by XRD (cf. Fig. 1) at the indicated reduction temperatures. $T_{reaction}$ = 523 K, $m_{catalyst}$ = 20 mg, $p_{CH3OH} = p_{H2O}$ = 30 mbar, total flow = 20 ml/min.

0.08 s^{-1}, respectively. The maximum achieved CO_2 selectivity is in agreement with previous studies of similar catalysts [14]. After reduction at 773 K, PdGa (1:1) is formed, which shows distinctly different catalytic properties than Pd_2Ga, characterized by a significantly decreased activity. Reoxidation of PdGa at 523 K followed by reduction at 673 K restores most of the previous activity, so the reason for the decrease in the activity is not simply particle sintering but the intrinsic catalytic properties of the PdGa intermetallic.

In the following, two points are of main interest: (i) the stability of the intermetallic (selective) catalytic surface and (ii) the origin of CO detected in the product stream.

3.3.1. Stability of the intermetallic surface

Our XRD studies have demonstrated that, concerning its bulk structure, the Pd_2Ga intermetallic is stable in air. IR spectroscopy, however, has indicated major changes in the outermost surface layer even upon room temperature exposure to oxygen (see Fig. 6(e2)). Starting from a catalyst in the CO_2 selective state (i.e., after reduction at 623 K), an exposure to air at room temperature results in a significantly decreased CO_2 selectivity and an accompanying decrease in total methanol conversion (see Fig. 8, right side). This confirms that although Pd_2Ga seems structurally stable in the bulk under these conditions (according to Ref. [34] even at higher temperature), the Pd_2Ga surface is indeed modified by oxygen already at room temperature and switches from a CO_2 selective state to one that exhibits catalytic properties closely resembling those of pure Pd. Interestingly, the activity after oxidative treatment is comparable to that after low-temperature reduction, which excludes the formation of a complete overlayer of oxidic Ga during the decomposition of the intermetallic. This indicates that the intensity losses observed upon oxidation in XP and IR spectroscopy are rather caused by islands of oxidic Ga that form upon decomposition of the intermetallic, but leave significant parts of the Pd surface accessible to reactants. Even a partial decoration of Pd by oxidic Ga is expected to reduce the overall reaction rate, however, as shown in Fig. 8, the CO_2 selectivity after oxidative treatment is still somewhat higher compared with the initial fully metallic state (T_{red} = 303 K), indicating that small parts of the surface remain intermetallic and contribute with their higher activity to the overall methanol conversion.

3.3.2. Origin of CO in the product stream

In agreement with previous studies [14], CO formation during MSR over Pd/Ga_2O_3 catalysts could only be suppressed to a certain extent (see Fig. 8). Two pathways are likely as source of CO production. One is methanol decomposition (MDC), as a possible parallel reaction to MSR, either on patches of metallic palladium or on the intermetallic compound itself. The other is the formation of CO by the reverse water–gas shift (RWGS) reaction from CO_2 and H_2 produced in MSR (i.e., a follow-up reaction). To identify the major CO formation mechanism, the activity of the Pd/Ga_2O_3 catalyst for reverse water–gas shift was determined under reaction conditions mimicking those during MSR, i.e., a feed composition with a molar ratio of CO_2:H_2 of 1:3, as is the expected composition in the MSR product stream. It turned out that RWGS activity is negligible under these conditions (see Fig. 9) and cannot explain the relatively large amounts of CO that are formed during MSR. Therefore, MDC is the likely source of CO production under steady-state reaction conditions. MDC occurs on metallic Pd detected during MSR reaction by IR spectroscopy (Fig. 7b). However, since directly after 673 K reduction no metallic Pd was detected at the surface (Fig. 6d), the small amounts of CO initially inducing partial decomposition of the IMC surface most likely originate either from MDC over the IMC itself or from RWGS on the support. The latter is supported by the fact that, under MSR conditions, the formation of CO beside CO_2 was also detected on the pure Ga_2O_3. The CO then restructures part of the surface, further increasing the MDC rate until an equilibrium state is reached.

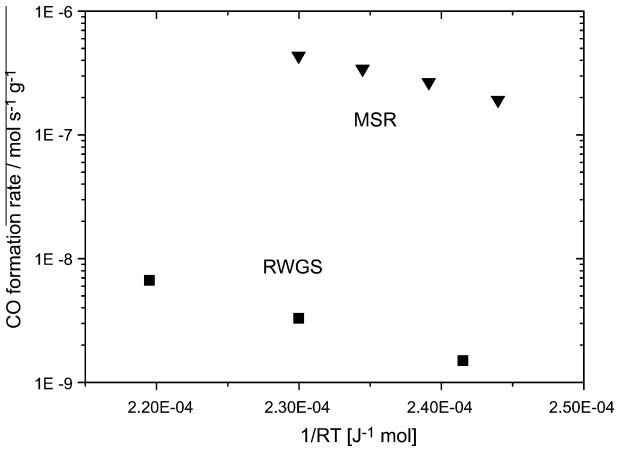

Fig. 9. Comparison of CO formation rates over 673 K-reduced Pd/Ga_2O_3 during MSR to those during RWGS. $m_{catalyst}$ = 20 mg, MSR: p_{CH3OH} = p_{H2O} = 10 mbar, RWGS: p_{CO2} = 18 mbar, p_{H2} = 54 mbar, total flow = 40 ml/min.

4. Conclusions

A range of *in situ* techniques of varying surface sensitivity were employed to study the formation and stability of intermetallic Pd–Ga compounds and the corresponding effects on catalytic properties in methanol steam reforming. It should be noted that the use of *in situ* techniques is particularly crucial for this system due to the dynamic response of the catalyst to the surrounding atmosphere.

In hydrogen, the formation of the bulk crystalline Pd_2Ga intermetallic compound starts at 548 K and is completed at 673 K. At the surface, however, modifications were observed already at temperatures as low as 423 K leading to beginning changes in activity and selectivity in MSR. Reduction at 773 K results in the formation of the Ga-richer IMC PdGa, which exhibits significantly lower activity in MSR.

While the nanoparticulate IMCs proved to be stable in air at room temperature regarding their bulk structure, their surface is affected by oxygen already at room temperature. Air exposure resulted in a decrease in MSR selectivity to values typical of metallic Pd, indicating decomposition of the IMC at the surface. Additionally, both IR and XPS point to a formation of Ga_xO_y islands, possibly by segregation of Ga from surface near regions to the outermost layer and subsequent oxidation.

Regarding stability, also CO was found to at least partially decompose the intermetallic surface. Exposure to CO led to the appearance of increasing amounts of bridge-bonded CO, characteristic of metallic Pd. Similarly, bridge-bonded CO was always observed by *in situ* IR spectroscopy during MSR. Thus, under reaction conditions, we assume that patches of metallic Pd are present at the surface, which are stabilized by CO. By catalyzing methanol decomposition to CO, these are most probably responsible for the significant amounts of CO detected in MSR product streams. Based on a comparison of reaction rates, reverse water–gas shift can rather be excluded as a main CO formation mechanism. Therefore, we suggest the presence of a dynamic equilibrium between intermetallic formation by H_2 and decomposition by CO. As a consequence, CO formation could not be fully avoided, due to the detrimental effect of CO on the selective Pd_2Ga intermetallic compound.

Acknowledgments

The authors acknowledge the beamtime granted at BESSY II at the ISISS beamline and support by the BESSY team. Dr. J. Bernardi and Dr. M. Stöger-Pollach (USTEM, TU Vienna) are acknowledged for TEM measurements. This work was financially supported by the Integrated Infrastructure Initiative I3 in FP6 Contract no. R II CT-2004-506008 and TU Vienna (IP VSFG). A.H. and K.F. acknowledge the Max Planck Society for research fellowships.

Appendix A. Supplementary material

Supplementary data associated with this article can be found, in the online version, at doi:10.1016/j.jcat.2011.10.007.

References

[1] D.R. Palo, R.A. Dagle, J.D. Holladay, Chem. Rev. 107 (2007) 3992.
[2] D.L. Trimm, Z.I. Onsan, Catal. Rev. – Sci. Eng. 43 (2001) 31.
[3] J.D. Holladay, Y. Wang, E. Jones, Chem. Rev. 104 (2004) 4767.
[4] S. Sá, H. Silva, L. Brandão, J.M. Sousa, A. Mendes, Appl. Catal., B 99 (2010) 43.
[5] G.A. Olah, Angew. Chem. Int. Ed. 44 (2005) 2636.
[6] H. Purnama, F. Girgsdies, T. Ressler, J.H. Schattka, R.A. Caruso, R. Schomäcker, R. Schlögl, Catal. Lett. 94 (2004) 61.
[7] B.A. Peppley, J.C. Amphlett, L.M. Kearns, R.F. Mann, Appl. Catal. A 179 (1999) 21.
[8] C.J. Jiang, D.L. Trimm, M.S. Wainwright, N.W. Cant, Appl. Catal. A 93 (1993) 245.
[9] B. Frank, F.C. Jentoft, H. Soerijanto, J. Kröhnert, R. Schlögl, R. Schomäcker, J. Catal. 246 (2007) 177.
[10] X. Cheng, Z. Shi, N. Glass, L. Zhang, J.J. Zhang, D.T. Song, Z.S. Liu, H.J. Wang, J. Shen, J. Power Sources 165 (2007) 739.
[11] T. Conant, A.M. Karim, V. Lebarbier, Y. Wang, F. Girgsdies, R. Schlögl, A. Datye, J. Catal. 257 (2008) 64.
[12] N. Iwasa, T. Mayanagi, W. Nomura, M. Arai, N. Takezawa, Appl. Catal. A 248 (2003) 153.
[13] M. Bäumer, J. Libuda, K.M. Neyman, N. Rösch, G. Rupprechter, H.J. Freund, Phys. Chem. Chem. Phys. 9 (2007) 3541.
[14] N. Iwasa, N. Takezawa, Top. Catal. 22 (2003) 215.
[15] N. Iwasa, T. Mayanagi, N. Ogawa, K. Sakata, N. Takezawa, Catal. Lett. 54 (1998) 119.
[16] A.P. Tsai, K. Satoshi, I. Yasushi, J. Phys. Soc. Jpn. 12 (2004) 3270.
[17] A. Bayer, K. Flechtner, R. Denecke, H.P. Steinruck, K.M. Neyman, N. Rosch, Surf. Sci. 600 (2006) 78.
[18] K.M. Neyman, K.H. Lim, Z.X. Chen, L.V. Moskaleva, A. Bayer, A. Reindl, D. Borgmann, R. Denecke, H.P. Steinruck, N. Rosch, Phys. Chem. Chem. Phys. 9 (2007) 3470.
[19] Z.X. Chen, K.M. Neyman, A.B. Gordienko, N. Rosch, Phys. Rev. B 68 (2003) 075417.
[20] T.B. Massalski, Binary Alloy Phase Diagrams, ASM International, Metals Park, OH, 1990.
[21] K. Kovnir, M. Armbrüster, D. Teschner, T.V. Venkov, F.C. Jentoft, A. Knop-Gericke, Y. Grin, R. Schlögl, Sci. Technol. Adv. Mater. 8 (2007) 420.
[22] J. Osswald, K. Kovnir, M. Armbrüster, R. Giedigkeit, R.E. Jentoft, U. Wild, Y. Grin, R. Schlögl, J. Catal. 258 (2008) 219.
[23] K. Kovnir, M. Armbrüster, D. Teschner, T.V. Venkov, L. Szentmiklósi, F.C. Jentoft, A. Knop-Gericke, Y. Grin, R. Schlögl, Surf. Sci. 603 (2009) 1784.
[24] M. Armbrüster, K. Kovnir, M. Behrens, D. Teschner, Y. Grin, R. Schlögl, J. Am. Chem. Soc. 132 (2010) 14745.
[25] G. Buckles, G.J. Hutchings, C.D. Williams, Catal. Lett. 8 (1991) 115.
[26] M. Barre, N.S. Gnep, P. Magnoux, S. Sansare, V.R. Choudhary, M. Guisnet, Catal. Lett. 21 (1993) 275.
[27] G.D. Meitzner, E. Iglesia, J.E. Baumgartner, E.S. Huang, J. Catal. 140 (1993) 209.
[28] N.S. Gnep, J.Y. Doyemet, A.M. Seco, F.R. Ribeiro, M. Guisnet, Appl. Catal. 43 (1988) 155.
[29] W. Jochum, S. Penner, K. Föttinger, R. Kramer, G. Rupprechter, B. Klötzer, J. Catal. 256 (2008) 268.
[30] W. Jochum, S. Penner, R. Kramer, K. Föttinger, G. Rupprechter, B. Klötzer, J. Catal. 256 (2008) 278.
[31] T. Mathew, Y. Yamada, A. Ueda, H. Shioyama, T. Kobayashi, C.S. Gopinath, Appl. Catal. A 300 (2006) 58.
[32] S.E. Collins, M.A. Baltanás, A.L. Bonivardi, J. Catal. 226 (2004) 410.
[33] S.E. Collins, M.A. Baltanás, J.L. Garcia Fierro, A.L. Bonivardi, J. Catal. 211 (2002) 252.
[34] S. Penner, H. Lorenz, W. Jochum, M. Stöger-Pollach, D. Wang, C. Rameshan, B. Klötzer, Appl. Catal. A 358 (2009) 193.
[35] H. Lorenz, S. Penner, W. Jochum, C. Rameshan, B. Klötzer, Appl. Catal. A 358 (2009) 203.
[36] H. Bluhm, M. Hävecker, A. Knop-Gericke, E. Kleimenov, R. Schlögl, D. Teschner, V.I. Bukhtiyarov, D.F. Ogletree, M. Salmeron, J. Phys. Chem. B 108 (2004) 14340.
[37] J.J. Yeh, I. Lindau, Atom. Data Nucl. Data Tables 32 (1985) 1.
[38] K. Kovnir, M. Schmidt, C. Waurisch, M. Armbrüster, Y. Prots, Y. Grin, Z. Kristallogr, NCS 223 (2008) 7.
[39] R. Carli, C.L. Bianchi, Appl. Surf. Sci. 74 (1994) 99.
[40] C.Y. Su, P.R. Skeath, I. Lindau, W.E. Spicer, Surf. Sci. 118 (1982) 248.
[41] B. Veisz, L. Tóth, D. Teschner, Z. Paál, N. Gyorffy, U. Wild, R. Schlögl, J. Mol. Catal. A: Chem. 238 (2005) 56.
[42] G. Rupprechter, Adv. Catal. 51 (2007) 133.
[43] N. Iwasa, S. Masuda, N. Ogawa, N. Takezawa, Appl. Catal. A 125 (1995) 145.
[44] H. Gabasch, W. Unterberger, K. Hayek, B. Klötzer, E. Kleimenov, D. Teschner, S. Zafeiratos, M. Hävecker, A. Knop-Gericke, R. Schlögl, J. Han, F.H. Ribeiro, B. Aszalos-Kiss, T. Curtin, D. Zemlyanov, Surf. Sci 600 (2006) 2980.
[45] H. Gabasch, E. Kleimenov, D. Teschner, S. Zafeiratos, M. Hävecker, A. Knop-Gericke, R. Schlögl, D. Zemlyanov, B. Aszalos-Kiss, K. Hayek, B. Klötzer, J. Catal. 242 (2006) 340.
[46] K. Zorn, S. Giorgio, E. Halwax, C.R. Henry, H. Grőnbeck, G. Rupprechter, J. Phys. Chem. C 115 (2010) 1103.
[47] O. Demoulin, G. Rupprechter, I. Seunier, B. Le Clef, M. Navez, P. Ruiz, J. Phys. Chem. B 109 (2005) 20454.
[48] K. Föttinger, J.A. van Bokhoven, M. Nachtegaal, G. Rupprechter, J. Phys. Chem. Lett. 2 (2011) 428.
[49] T. Lear, R. Marshall, J.A. Lopez-Sanchez, S.D. Jackson, T.M. Klapotke, M. Bäumer, G. Rupprechter, H.-J. Freund, D. Lennon, J. Chem. Phys. 123 (2005) 174706.
[50] T. Dellwig, J. Hartmann, J. Libuda, I. Meusel, G. Rupprechter, H. Unterhalt, H.J. Freund, J. Mol. Catal. A: Chem. 162 (2000) 51.
[51] W. Sachtler, Le Vide 164 (1973) 67.
[52] E.W. Plummer, W.R. Salaneck, J.S. Miller, Phys. Rev. B 18 (1978) 1673.
[53] C. Rameshan, W. Stadlmayr, C. Weilach, S. Penner, H. Lorenz, M. Hävecker, R. Blume, T. Rocha, D. Teschner, A. Knop-Gericke, R. Schlögl, N. Memmel, D. Zemlyanov, G. Rupprechter, B. Klötzer, Angew. Chem. Int. Ed. 49 (2010) 3224.
[54] Y. Soma-Noto, W. Sachtler, J. Catal. 32 (1974) 315.
[55] M. Primet, M.V. Mathieu, W.M.H. Sachtler, J. Catal. 44 (1976) 324.
[56] H. Gabasch, A. Knop-Gericke, R. Schlögl, M. Borasio, C. Weilach, G. Rupprechter, S. Penner, B. Jenewein, K. Hayek, B. Klötzer, Phys. Chem. Chem. Phys. 9 (2006) 533.
[57] S. Tanuma, C.J. Powell, D.R. Penn, Surf. Interface Anal. 17 (1991) 911.